Earthquake Engineering & Structural Dynamics
The Journal of the International Association for Earthquake Engineering

EARTHQUAKE ENGINEERING & STRUCTURAL DYNAMICS
Earthquake Engng Struct. Dyn. 2016:1–20
Published online in Wiley Online Library (wileyonlinelibrary.com). DOI: 10.1002/eqe.2716

Evaluation of seismic performance of pile-supported models in liquefiable soils

D. Lombardi[1,*,†] and S. Bhattacharya[2]

[1]*School of Mechanical, Aerospace and Civil Engineering, The University of Manchester, Manchester, UK*
[2]*Department of Civil and Environmental Engineering, University of Surrey, Guildford, UK*

SUMMARY

The seismic performance of four pile-supported models is studied for two conditions: (i) transient to full liquefaction condition, i.e. the phase when excess pore pressure gradually increases during the shaking; (ii) full liquefaction condition, i.e. defined as the state where the seismically induced excess pore pressure equalises to the overburden stress. The paper describes two complementary analyses consisting of an experimental investigation, carried out at normal gravity on a shaking table, and a simplified numerical analysis, whereby the soil–structure interaction (SSI) is modelled through non-linear Winkler springs (commonly known as *p–y* curves). The effects of liquefaction on the SSI are taken into account by reducing strength and stiffness of the non-liquefied *p–y* curves by a factor widely known as *p-multiplier* and by using a new set of *p–y* curves. The seismic performance of each of the four models is evaluated by considering two different criteria: (i) strength criterion expressed in terms of bending moment envelopes along the piles; (ii) damage criterion expressed in terms of maximum global displacement. Comparison between experimental results and numerical predictions shows that the proposed *p–y* curves have the advantage of better predicting the redistribution of bending moments at deeper elevations as the soil liquefies. Furthermore, the proposed method predicts with reasonable accuracy the displacement demand exhibited by the models at the full liquefaction condition. However, disparities between computed and experimental maximum bending moments (in both transient and full liquefaction conditions) and displacement demands (during transient to liquefaction condition) highlight the need for further studies. Copyright © 2016 The Authors Earthquake Engineering & Structural Dynamics Published by John Wiley & Sons Ltd.

Received 5 June 2015; Revised 14 January 2016; Accepted 18 January 2016

KEY WORDS: soil liquefaction; piles; seismic performance; shaking table; winkler springs

1. INTRODUCTION

Post-earthquake site investigations have confirmed that liquefaction still represents one of the predominant causes of damage to structures after major earthquakes [1–7]. Despite the extensive research in this field, effects induced by liquefaction on the soil–structure interaction (SSI) are still uncertain and inadequately addressed by modern seismic codes [8–10]. In this context, one of the critical aspects of the design consists of a realistic assessment of the seismic performance of structures during and immediately after the onset of soil liquefaction.

In routine practice, the seismic design of pile-supported structures is based on the assumption that the action exerted by an earthquake can be represented by equivalent static forces that are proportional to the mass of the structure and spectral acceleration. Such an approach, which is normally referred to as force-based design because the seismic demand is expressed in terms of a pseudo-static force, requires as input parameters three modal structural properties, namely: vibration

*Correspondence to: School of Mechanical, Aerospace and Civil Engineering, The University of Manchester, Manchester, UK
†E-mail: domenicolombardi@gmail.com, domenico.lombardi@manchester.ac.uk

period, equivalent viscous damping and ductility capacity. Based on these structural parameters, the acceleration required for the assessment of the base shear force can be determined from an idealised acceleration response spectrum, such as the one depicted in Figure 1. In a conventional force-based design, the effects induced by soil liquefaction, namely lengthening in period [11, 12] and increase in damping ratio, which can reach value as high as 20%, see for example [11], have significant consequences on the assessment of the seismic demand imposed by the shaking. Lombardi & Bhattacharya [11] concluded that the pseudo-acceleration, and consequently the base-shear force, that the structure would experience during liquefaction condition may be significantly lower than that experienced prior to liquefaction condition (see Figure 1). This apparent beneficial effect (i.e. reduction in seismic demand) experienced by pile-supported structures during liquefaction conditions suggests that it might be questionable whether the performance of a structure founded in liquefiable soils can be realistically assessed through a conventional force-based design approach. As a result, this is still an area of active research.

This paper aims to evaluate the seismic performance of four pile-supported structures under two conditions. These are hereafter referred to as: (i) *transient to liquefaction condition*, which may be defined as the phase when excess pore pressure gradually increases with shaking till full liquefaction is reached; (ii) *full liquefaction condition*, which corresponds to the state where the seismically induced excess pore pressure equalises the overburden geostatic stress. The seismic performance of four models representing typical pile-supported structures is evaluated against two different criteria, namely: (i) strength criterion, which is being assessed through maximum bending moment envelopes along the piles; (ii) damage criterion which is being related to material strain but conveniently expressed in terms of maximum global displacement of the models. The work comprises two complimentary studies, consisting of:

1. Experimental investigation carried out at normal gravity on a shaking table, whereby a 1.7-m-high soil deposit is gradually liquefied by the base shaking and the dynamic behaviour of four pile-supported structures is continuously monitored by means of accelerometers and strain gauges.
2. Numerical analyses in which the SSI is modelled by means of discrete spring, i.e. *p–y* curves, according to the Winkler approach. The effects induced by liquefaction on the SSI are taken into account by reducing the initial stiffness and strength of the non-liquefied *p–y* curves according to the *p-multiplier approach* and by means of novel *p–y* curves proposed by the authors. Differently

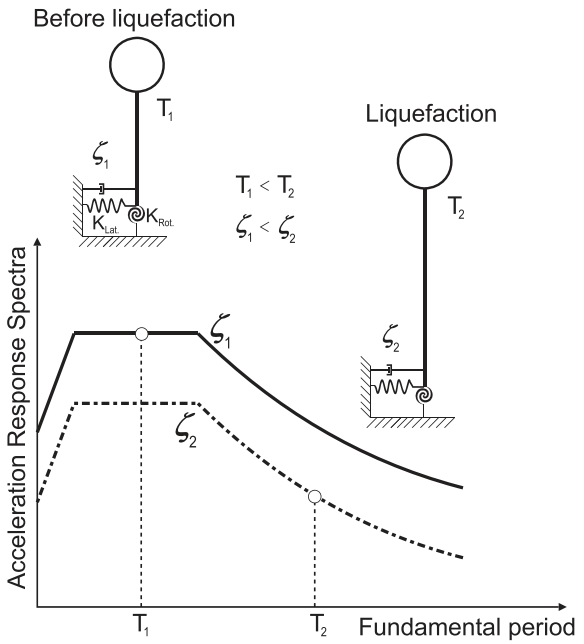

Figure 1. Effects of liquefaction on acceleration response spectrum (redrawn from [13]).

DOI: 10.1002/eqe

from the existing *p–y* curves for liquefiable soils (these are constructed according to the *p-multiplier* method), the proposed relationships have the advantage of replicating the actual strain hardening, and dilative behaviour, exhibited by the liquefied soil when sheared in undrained conditions as result of pile–soil relative displacement. The bending moment envelopes are computed based on the conventional pseudo-static approach, whereby the seismic action is represented by a base-shear force that is proportional to the mass and pseudo-acceleration of the model. The computed bending envelopes are compared against those measured from strain data recorded on the instrumented piles. The global maximum displacements are computed graphically according to the capacity-spectrum method from the intersection points between capacity and seismic demand curves plotted in acceleration–displacement format. The computed maximum global displacements are finally compared against displacement time histories computed by double integration of acceleration measurements with respect to time.

Before presenting the main research carried out by the authors, the paper reviews current methods for pile design in liquefiable soils and existing *p–y* curves for liquefiable soils. Subsequently, the authors discuss the need for a new generation of *p–y* curves for liquefiable soils.

2. CURRENT METHODS FOR PILE ANALYSIS AND DESIGN IN LIQUEFIABLE SOILS

The Japanese Highway Code of practice [14] advises practising engineers to consider two different loading conditions, namely: (i) kinematic load exerted by the lateral pressure of the liquefied layer and/or any non-liquefied crust resting on the top of the liquefied deposit; (ii) inertial load because of the oscillation of the superstructure. The code also recommends checking against bending failure because of kinematic and inertia loads, separately. Similarly, Eurocode 8 [8] advises engineers to design piles against bending because of inertia and kinematic loads arising from the deformation of the surrounding soil. In the event of liquefaction, however, Eurocode 8 [8] also recommends that '*the side resistance of soil layers that are susceptible to liquefaction or to substantial strength degradation shall be ignored*'. Other provisions, such as the NEHRP code and Indian Code [9, 10], adopt similar approaches that are all based on the bending failure mechanism. In summary, it can be concluded that the current codes of practice treat pile as laterally loaded beams, which may be prone to bending failures.

Recent studies [15–20] suggest an alternative failure mechanism, whereby end-bearing piles act as unsupported long slender columns owing to the loss of stiffness and strength of the liquefied layer, which may become unstable and buckle under the action of large axial loads exerted by the superstructure. According to this failure mechanism, piles would be better modelled by means of beam-column elements carrying both lateral and axial loads rather than laterally loaded beams, as adopted in current routine practice. Such a method would be also in agreement with '*Principle P(4)*' stated in section 5.4.2 of Eurocode 8-Part 5 [21], which advices engineers to ignore the side resistance offered by layers susceptible to liquefaction or substantial degradation. Evidently, such an assumption implies that piles would be better modelled as free-standing columns that extend to the entire liquefiable layer and fixed at some depth into the non-liquefiable soil [11, 22].

2.1. *Brief review of p–y* curves for modelling SSI in liquefiable soils

Most of the numerical methods currently in use for modelling SSI are based on the *Beam on Elastic Foundation approach* [23]. This approach is based on the hypothesis that the reaction forces exerted by the foundation are proportional at every point to the deflection of the pile at that point and are independent of pressures or deflections produced elsewhere in the foundation. The factor of proportionality between the soil resistance, p (with units of *force/displacement*^{2}), and pile–soil relative displacement, y, is normally referred to as *coefficient of subgrade reaction*, k_s (with units of *force/length*^{3}).

$$p = k_s y \tag{1}$$

DOI: 10.1002/eqe

Over the past years, nonlinear *p–y* curves have been extensively used in the offshore industry. Specifically, institutions such as the *American Petroleum Institute* [24] and *Det Norske Veritas* [25] provide procedures for the construction of nonlinear *p–y* curves for sandy and clayey soils separately. It is worth noting that these procedures have been developed based on a limited number of tests carried out on full-scale small diameter steel piles subjected to slow-cyclic loading [26, 27]. As a result, it is questionable whether these *p–y* curves can be adopted to model SSI in liquefiable soils because the latter is strongly dependent upon the loss of strength and stiffness because of excess pore pressure build-up.

One of the first attempts to develop *p–y* curves for laterally loaded piles in liquefiable soils is presented by Dobry *et al*. [28]. The proposed method consists of multiplying the conventional *p–y* curves for sandy soils by a degradation factor m_p that is referred to as *p-multiplier*. As shown in Figure 2, m_p decreases almost linearly with increasing excess pore pressure, attaining a limiting value of $m_p = 0.1$ at the full liquefaction condition [29–31]. Other studies recommend values of m_p ranging from 1/80 to 1/30 (see for example Cubrinovski *et al*. [32]) or express m_p as a function of blow counts obtained from standard penetration SPT tests [33, 34]. It should be noted that the disparities between the different values proposed for m_p by different researchers can be probably attributed to numerous uncertainties associated with the procedures used for back-calculating m_p. More details regarding the *p-multiplier* approach can be found in Finn [35].

A different method for modelling *p–y* curves during liquefaction condition is based on the assumption that the liquefied soil behaves as a soft clay. According to this approach, the *p–y* curves can be obtained from the ones recommended by the *American Petroleum Institute* [24] for soft clays, but replacing the undrained shear strength with the residual strength of the liquefied soil, S_r [36, 37]. The existing *p–y* curves for liquefiable soils imply a significant stiffness in the initial phase of pile–liquefied soil interaction, which is followed by strain-softening response. However, this response is in contrast with recent studies [30, 38–41] that showed that the undrained response of liquefied sands is strain hardening. This is characterised by practically zero stiffness at low strains and increasing stiffness upon shearing. This unusual strain-hardening response can be attributed to the tendency of the liquefied soil to dilate upon shearing. In fact, as the liquefied soil tends to dilate, the excess pore pressure gradually dissipates, which in turn leads to an increasing strength and stiffness upon shearing.

In view of these recent findings, this paper adopts a new set of *p–y* curves that can be obtained by modifying the conventional *p–y* curves (for nonliquefied soils) in such a way to replicate the strain-hardening behaviour aforementioned. A comparison between the proposed *p–y* curves and those obtained according to the *p-multiplier* method is plotted in Figure 3. In the following sections, the application of both conventional and modified *p–y* curves is illustrated by means of a series of

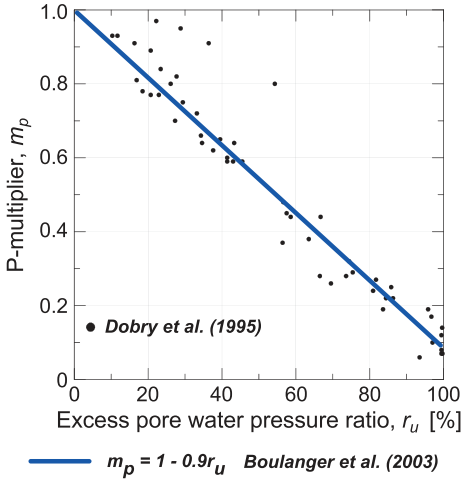

Figure 2. *p-multiplier* versus excess pore pressure ratio (redrawn from Boulanger et al. [29]).

DOI: 10.1002/eqe

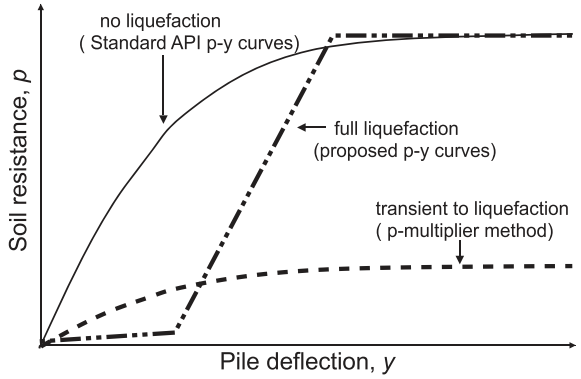

Figure 3. Comparison between conventional and proposed p–y curves for liquefied soils.

numerical analysis whose results are compared against experimental data obtained from large-shaking table tests.

3. EXPERIMENTAL INVESTIGATION: SHAKING TABLE TESTS AND INSTRUMENTATION

An experimental investigation is carried out in the shaking table facility of the Bristol Laboratory for Advanced Dynamics Engineering (BLADE) at the University of Bristol (UK). The tests are performed at normal gravity on physical models representing two single piles (Model ID: SP1 and SP2) and two 2×2 pile groups (Model ID: GP1 and GP2) structures. Aluminium alloy (type L114-T4 6082-T4) is selected as material for all piles. The latter are cut into tubes of 2 m long and rigidly connected to a bottom plate so as to guarantee bottom-fixed conditions for all models. This condition can be assumed valid when piles penetrate into firm soil layers, which are not susceptible to liquefaction condition. Each model is equipped with a rigid pile-cap fabricated using steel plates. In the pile group models, the presence of this rigid cap implies fixity conditions at the top of the piles. The dimensions and mechanical properties of the models are listed in Table I. A photograph of the experimental apparatus used in the tests is given in Figure 4(a), and a schematic of the instrumentation layout is depicted in Figure 4(b). The soil container consists of a rigid box made of steel with dimensions of 2.4-m length, 2.4-m height and 1.2-m width. To reduce the effects body wave generation and reflection from the artificial boundaries, the inner sides of the container are fitted with conventional foams which act as absorbing materials. More details regarding the selection of the foam and thickness of the absorbing boundaries can be found in [42]. The sand deposit is made of uniform layers of Redhill 110 sand that are pluviated from a constant height of fall of 1.5 m. The saturation of the soil deposit is achieved from top to bottom. This is monitored through a set of pore pressure transducers (PPTs) whose location is illustrated in Figure 4(b). The final value of relative density is about 34%. The input acceleration and acceleration responses of the models are monitored by means of accelerometers located on the table and pile-caps, respectively. Each pile is instrumented with pairs of strain gauges mounted at four different elevations, which are subsequently used to derive bending moment profiles. The data acquisition system consists of 4

Table I. Dimensional and mechanical properties of the models.

Model ID	Outer diameter [mm]	Thickness [mm]	EI pile [Nm^2]	Pile-cap dimensions [mm]	Pile-cap weight [kg]
SP1	25.4	0.711	294	$100 \times 100 \times 25.4$	1.9
SP2	41.275	0.711	1305	$150 \times 150 \times 25.4$	8.44
GP1	25.4	0.711	294	$260 \times 260 \times 25.4$	13.08
GP2	41.275	0.711	1305	$260 \times 260 \times 25.4$	22.72

DOI: 10.1002/eqe

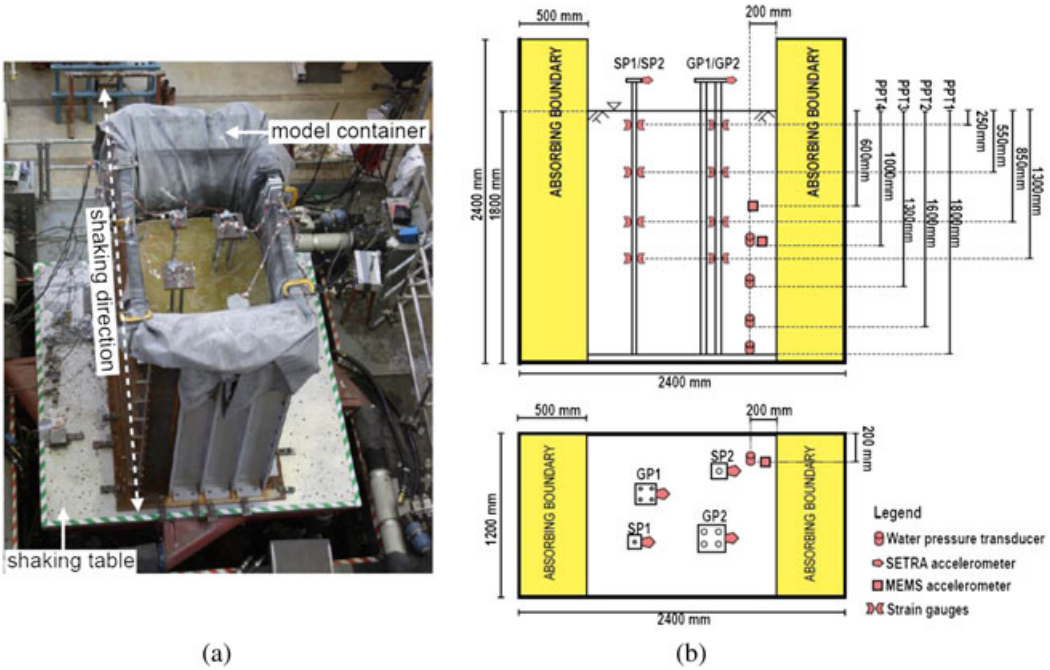

Figure 4. Experimental apparatus: (a) photograph of the experimental apparatus; (b) schematic representation of the experimental set-up and instrumentation layout.

Microstar Laboratories MSXB028 analog–digital converter (ADC) cards having 64 channels. Data is simultaneously sampled at a target frequency of 200 Hz and filtered with a low pass Butterworth filter set at 80 Hz.

The input motion consists of a white noise signal having bandwidth frequency ranging from 0 to 100 Hz. Three levels of acceleration, i.e. 0.02 g, 0.04 g and 0.15 g, are applied through the shaking table. Each level of acceleration is applied for 100 s, and it is swiftly incremented without stopping the shaking, which has a total duration of 300 s. As depicted in Figure 5, each value of acceleration corresponds to a different factor of safety *FOS* against liquefaction [43]. The latter is being defined as ratio of cyclic resistance ratio *CRR* to cyclic stress ratio *CSR*. Based on this definition, liquefaction is expected to be triggered when FOS < 1:

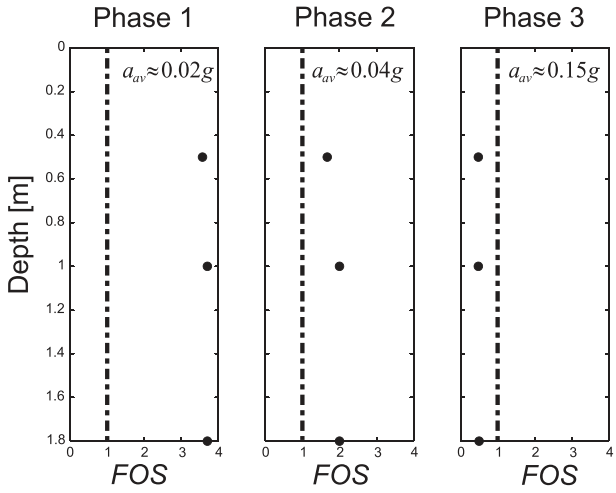

Figure 5. Factor of safety *FOS* against liquefaction attained in the three different phases of the shaking.

DOI: 10.1002/eqe

$$FOS = \frac{CRR}{CSR}. \tag{2}$$

The value of *CRR* has been estimated by means of element tests whose results are presented and discussed by the authors in [38]. The cyclic stress ratio *CSR* is a function of the depth z; hence, it may vary within the soil deposit. In this study, *CSR* is computed by using the expression suggested by Seed & Idriss [43], and recommended by EC8 [21].

$$CSR = 0.65 r_d \frac{\sigma_{v0}}{\sigma'_{v0}} \frac{a_{\max}}{g}, \text{where} r_d = 1 - 0.012z \tag{3}$$

The onset of liquefaction condition is attained when the excess pore pressure r_u, defined as the ratio of excess pore pressures to overburden effective stress, reaches a value close to unity. Prior to this, the condition of incremental excess pore pressure build-up is hereafter referred to as transient condition (see Figure 6).

Figure 7 plots the acceleration time histories measured on the pile-caps of the four models. It can be observed that the acceleration responses exhibited by the models reduce with increasing excess pore pressure, owing to significant soil softening because of excess pore pressure build-up.

Figure 8 plots the displacement time histories of the four models. These are computed from accelerometers located on the pile-caps by means of numerical (double) integration of the recorded accelerometer signals. To minimise potential errors inherent to the numerical integration [44], the input data is filtered through a digital fourth-order Butterworth filter with highpass and lowpass frequencies set at 1 Hz and 80 Hz, respectively. The displacement–time histories show that, during the transient to liquefaction, the displacement response of the four models amplifies with respect to that of the table. The latter has been denoted by darker lines in the same figure. On the other hand, as the excess pore pressure gradually increases, the displacement amplification (defined as ratio of model to table response) gradually reduces, attaining a value close to unity at the full liquefaction condition.

The pseudo elastic response spectra depicted in Figure 9 are computed based on the acceleration time history recorded by the accelerometer located 600 mm below the ground level (see Figure 4(b)). Specifically, the response spectrum for the transient condition is estimated based on the acceleration time history recorded during the so-called transient phase (see Figure 7) and considering an equivalent viscous damping of 7%. The latter is an average value estimated from a series of free-vibration tests carried out on the models before the application of the shaking. The

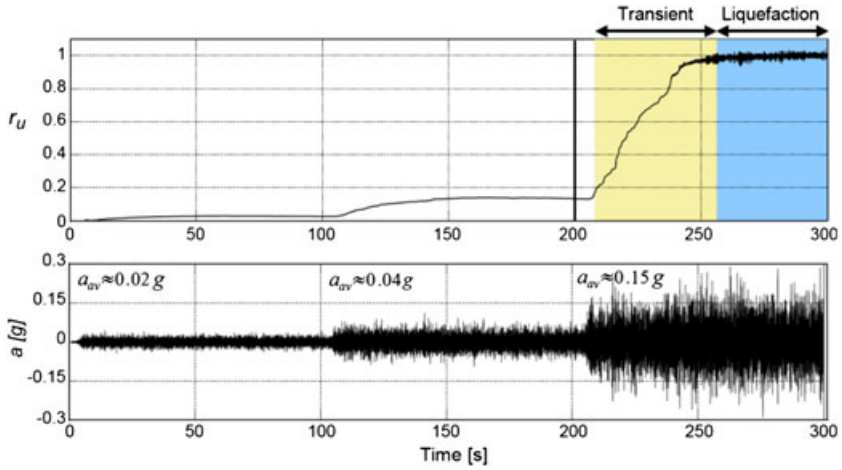

Figure 6. Input time–acceleration history (recorded on the table) and corresponding excess pore pressure ratio r_u. (full liquefaction condition is attained when r_u~1).

DOI: 10.1002/eqe

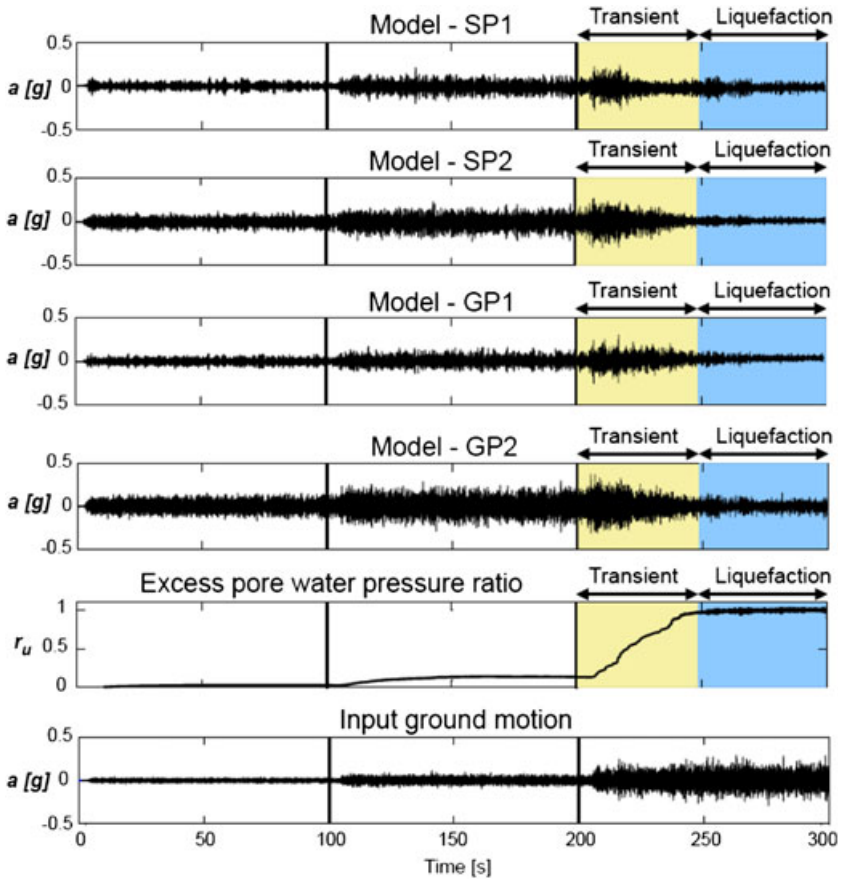

Figure 7. Acceleration responses of models (recorded on the pile-caps), excess pore pressure and input ground motion time histories.

pseudo-acceleration response spectrum for the full liquefaction condition is determined from the acceleration time history recorded after r_u attained a value of 1 (see Figure 7) and for an effective viscous damping of 20%. This corresponds to the average value of viscous damping exhibited by the four models at the full liquefaction conditions, whereby the damping of each model is computed according to the 'Half-Power Bandwidth' method [45]. More details regarding the system identification techniques used for the assessment of the modal parameters of each model (i.e. natural frequency and viscous damping) can be found in [11]. It is worth noting that the greater value of damping computed during liquefaction condition is consistent with the higher dissipation of energy that is expected because of the combined effects because of hysteretic behaviour of the liquefied soil and wave radiation. Furthermore, the use of an effective damping that is greater than the conventional value of 5% is also advocated by major seismic provisions (e.g. Eurocode 8) in the presence of structures founded in very soft soil deposits (this acts as a base isolator), such as liquefiable soils, and/or in presence of significant SSI effects.

4. NUMERICAL ANALYSIS

The seismic behaviour of the four models tested on the shaking table is investigated numerically in the finite element software *SAP2000*, *V 14* [46]. The piles are modelled by means of beam-column elements having structural properties and boundary conditions equivalent to those of the physical models described in Section 3. The pile-caps are modelled by lumped masses applied in the translational degrees of freedom and setting to zero masses for the rotational degrees of freedom.

DOI: 10.1002/eqe

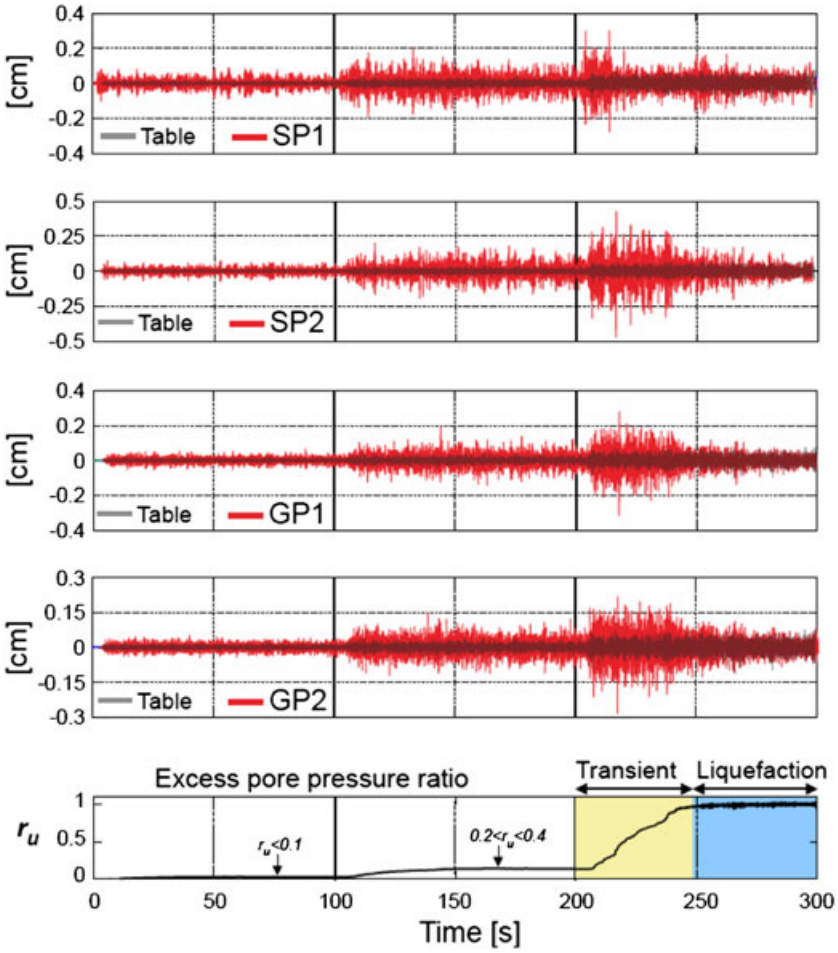

Figure 8. Displacement responses of models (recorded on the pile-caps), input displacement (recorded on the table) excess pore pressure time histories.

For pile-group models, i.e. GP1 and GP2, the restrained conditions imposed by the pile-caps are modelled by means of diaphragm constraints, whereby all joints within the pile-cap move together as a planar rigid diaphragm. Effects because of geometric nonlinearities are taken into account in the

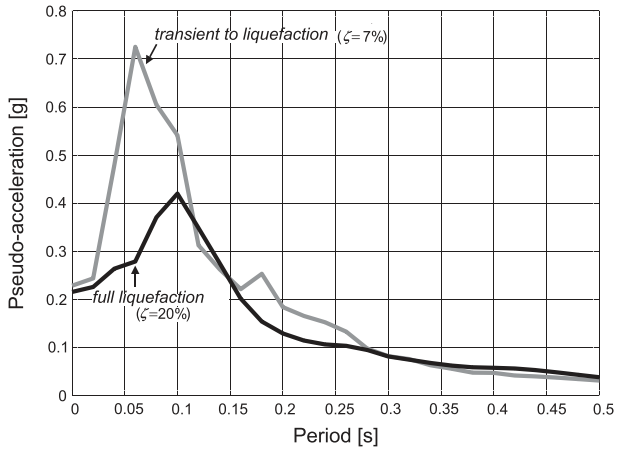

Figure 9. Elastic pseudo-acceleration response spectra computed in transient and full liquefaction conditions.

DOI: 10.1002/eqe

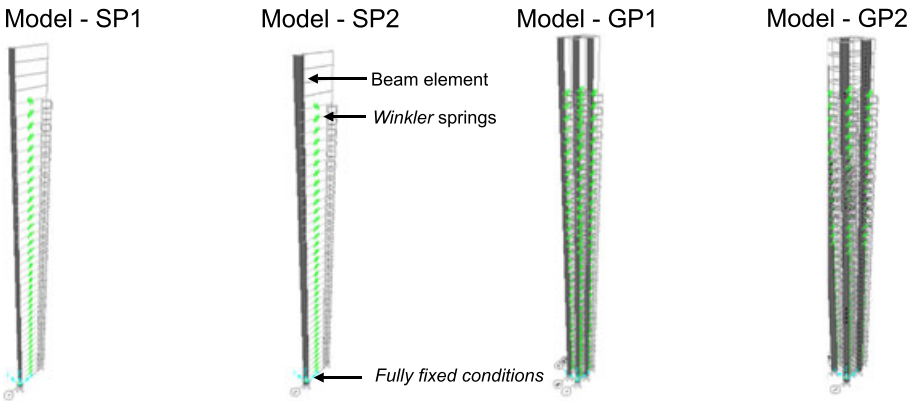

Figure 10. Numerical models.

form of P-delta effects. This implies that all equilibrium equations are solved considering the deformed configurations of the models.

The SSI is modelled by means of discrete springs according to the Winkler approach described in Section 2.1 As shown in Figure 10, each spring is attached to the beam-column element through the so-called 'link element' available in SAP2000 [46]. Each link element is defined by two joints connected to the beam-column element and a restraint, respectively. The individual 'link element' is defined by an appropriate nonlinear soil resistance-displacement relationship, i.e. p–y curve. The latter is constructed according to the hyperbolic function recommended by the American Petroleum Institute [24] given by:

$$p = Ap_u \tanh\left(\frac{k_s H}{Ap_u} \cdot y\right) \tag{4}$$

where A is a factor that accounts for the cyclic nature of the loading. This is taken equal to 0.9 according to API code [24]; p_u denotes the ultimate lateral bearing capacity. At a given depth H, p_u is computed as the smallest value between $(C_1H + C_2D)\gamma' H$ and $C_3D\ \gamma' H$. The coefficients C_1, C_2 and C_3 are determined according to the API code [24] as a function of the angle of shearing resistance of the sand in its non-liquefied state. Similarly, the coefficient of subgrade reaction, k_s, is determined from empirical relationships as a function of the angle of shearing resistance of the non-liquefied soil. In this study all parameters are determined based on the critical angle of the sand used in the shaking table test (i.e. Redhill 110), which is 36° after Lombardi [47]. The use of a critical state parameter is not only a convenient choice because this is independent of the particular soil conditions (e.g. excess pore pressure, stress state, strain level, etc.), its use can also be justified considering the relatively high strain levels attained during the shaking.

4.1. p–y curves for transient to liquefaction condition

During the transient to liquefaction condition (i.e. $r_u < 1$), the p–y curves exhibit conventional elasto-plastic response characterised by reducing strength and stiffness upon shearing. These are formulated based on the hyperbolic expression given by (4), but applying a reduction factor that takes into account the reduction in strength and stiffness induced by the excess pore pressure build-up. It is important to note, however, that the degradation factor used in the transient condition is lower than that used at the full liquefaction condition (see Section 4.2). In fact, in this condition the degradation factor is determined based on an iterative procedure by which the reduction factor is gradually reduced until a match between the numerically computed and experimental frequencies of the models is achieved. The computed reduction factors and corresponding computed and measured frequencies are listed in Table II. More details regarding the system identification techniques used for the assessment of the natural frequencies of the physical models can be found in [11]. In the absence of experimental data, an alternative method to estimate the reduction factor during the transient to liquefaction condition

DOI: 10.1002/eqe

Table II. Reduction factor for transient to liquefaction condition and comparison between measured and numerically computed frequencies

Model ID	Reduction factor	Measured [Hz]	Numerical [Hz]
SP1	0.7	4.41	4.14
SP2	0.2	3.46	3.46
GP1	0.5	5.04	5.02
GP2	0.3	6.13	6.13

consists of using the linear function proposed by Boulanger *et al*. [29], which is depicted in Figure 2. A direct comparison between the two procedures would be inappropriate because the values of reduction factor used in the present study are estimated for r_u ranging from 0.2 to 0.9 (this identifies the so-called transient condition, see Figure 6) whereas the linear function would estimate the m_p for a given value of r_u.

4.2. *p–y* curves for full liquefaction condition

To model the effects of liquefaction on the SSI, two different types of *p–y* curves are used: (i) *p–y* curves modified according to the *p-multiplier approach*, whose limitations are highlighted in Section 2.1; (ii) new proposed *p–y* curves.

4.2.1. p-multiplier approach:. The *p-multiplier* used to construct *p–y* curves for liquefied conditions is back-calculated based on an iterative procedure in which m_p is gradually reduced until a match between the experimental and numerically computed frequencies of the models is achieved. The computed *p-multipliers* and the frequencies used in this iterative procedure are listed in Table III. It is worth noting that these *p-multipliers* are consistent with values reported in the literature that have been presented in Section 2.1.

4.2.2. Proposed p–y curves. A reliable *p–y* relationship has to be consistent with the response of liquefied samples as observed in both soil element and physical model tests. As discussed in Section 2.1, this response is characterised by a strain-hardening behaviour whereby the soil is initially sheared at practically zero stiffness but, once exceeding a threshold value of strain, it starts to mobilise increasing strength and stiffness upon shearing. This behaviour is associated with the tendency of the liquefied soil to dilate, which in the undrained condition, results in a gradual dissipation of excess pore pressure and subsequent increase in strength and stiffness of the liquefied soil. The threshold strain upon which the liquefied soil exhibits a tendency to dilate, and thus mobilises non-zero strength and stiffness, is hereinafter referred to as take-off strain, denoted by γ_{to}. In a recent study conducted by Lombardi *et al* [38], it was found that for two different silica sands, i.e. Toyoura and Redhill 110, γ_{to} is predominantly a function of the initial relative density of the soil. This is in agreement with fundamental soil mechanics in which the tendency to dilate of a given soil (at a certain level of confinement, i.e. certain depth) is related to its initial degree of packing. Figure 11 shows typical results obtained from multi-stages cyclic triaxial tests carried out on samples of silica sands. It may be seen that γ_{to} increases with decreasing relative density, which suggests that denser soils mobilise non-zero strength and stiffness at lower strains. Lombardi *et al* [38] provided an empirical relationship between γ_{to} and D_r, which is here re-proposed:

Table III. *p-multiplier* for full liquefaction condition and comparison between measured and numerically computed frequencies.

Model ID	m_p	Measured [Hz]	Numerical [Hz]
SP1	0.3	3.77	3.72
SP2	0.1	2.18	2.10
GP1	0.1	4.28	4.17
GP2	0.1	4.35	4.32

DOI: 10.1002/eqe

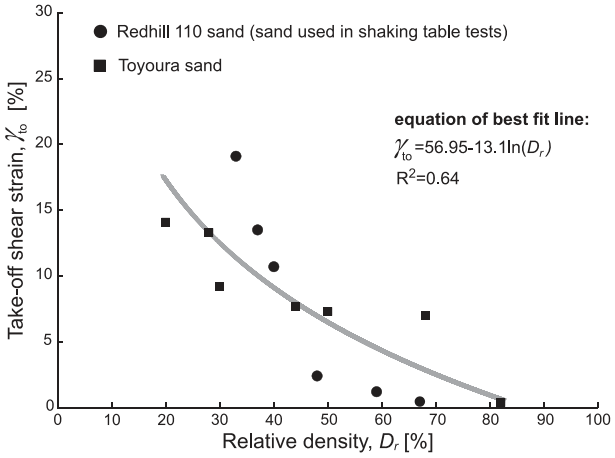

Figure 11. Results from cyclic triaxial tests plotting the shear strain required to mobilise 1 kPa of shear stress (referred to as take-off shear strain), γ_{to}, versus initial relative densities (modified after Lombardi *et al*. [38]).

$$\gamma_{to} = 56.95 - 13.1\ln(Dr) \quad \text{where } D_r \text{is expressed in } \%. \tag{5}$$

The construction of the proposed *p–y* curves for liquefied soils requires four parameters. These are:

1. take-off displacement y_{to}. As shown in Figure 12(a), this can be determined by converting the corresponding take-off strain γ_{to} (determined from Figure 11) into an equivalent displacement y_{to}, such that:

$$y_{to} = \frac{\gamma_{to} D}{M_S} \tag{6}$$

where M_S is a scaling factor used to convert strain into displacement and D is the diameter of the pile. In this study M_S is taken as 1.87 after Dash [39] and Bouzid *et al*. [48]. Table IV lists the values of y_{to} computed for this numerical investigation.

1. initial subgrade reaction (stiffness) mobilised at $y \leq y_{to}$. Experimental results presented by Lombardi *et al*. [38] showed very low values of initial shear modulus of the liquefied soil for $\gamma < \gamma_{to}$. Specifically, for samples of Redhill 100 sand prepared at a relative density of 34% (i.e. relative density achieved in the shaking table tests) the initial shear modulus is about 5 kPa. As a result, the initial subgrade reaction for $y \leq y_{to}$ is set to practically zero although a non-zero value of 1 kPa has been used to avoid numerical errors.
2. subgrade reaction mobilised at $y > y_{to}$. As schematically depicted in Figure 12(a), the *p–y* relationship beyond y_{to} is increasing linearly with increasing displacements. As a result, a single value of subgrade reaction is required for the construction of *p–y* response for $y > y_{to}$. Experimental evidence [38, 39] indicates that the post-liquefied stiffness is mainly function of the initial relative density of the soil and comparable to that the same soil would exhibit in its non-liquefied state. As a result, the subgrade reaction mobilised at $y > y_{to}$ is taken equal to that used in the hyperbolic function given by (4) and defined in Section 4.
3. ultimate soil resistance p_u. This is taken equal to the ultimate lateral bearing capacity as previously defined by (4), and it is justified by the fact that the post-liquefied behaviour of the soil is mainly function of the initial relative density of the soil.

Typical examples of *p–y* curves for liquefied soils used in this study are shown in Figure 12(b).

4.3. Pseudo-static analysis: seismic performance based on strength (bending) criterion

The aim of the pseudo-static analysis is to evaluate the seismic performance of the four models based on a strength-type performance criterion. This is normally expressed in terms of maximum bending moment diagrams. To assess the reliability of the numerical models, the computed bending moment envelopes are compared against bending moment profiles estimated from experimental data. The

DOI: 10.1002/eqe

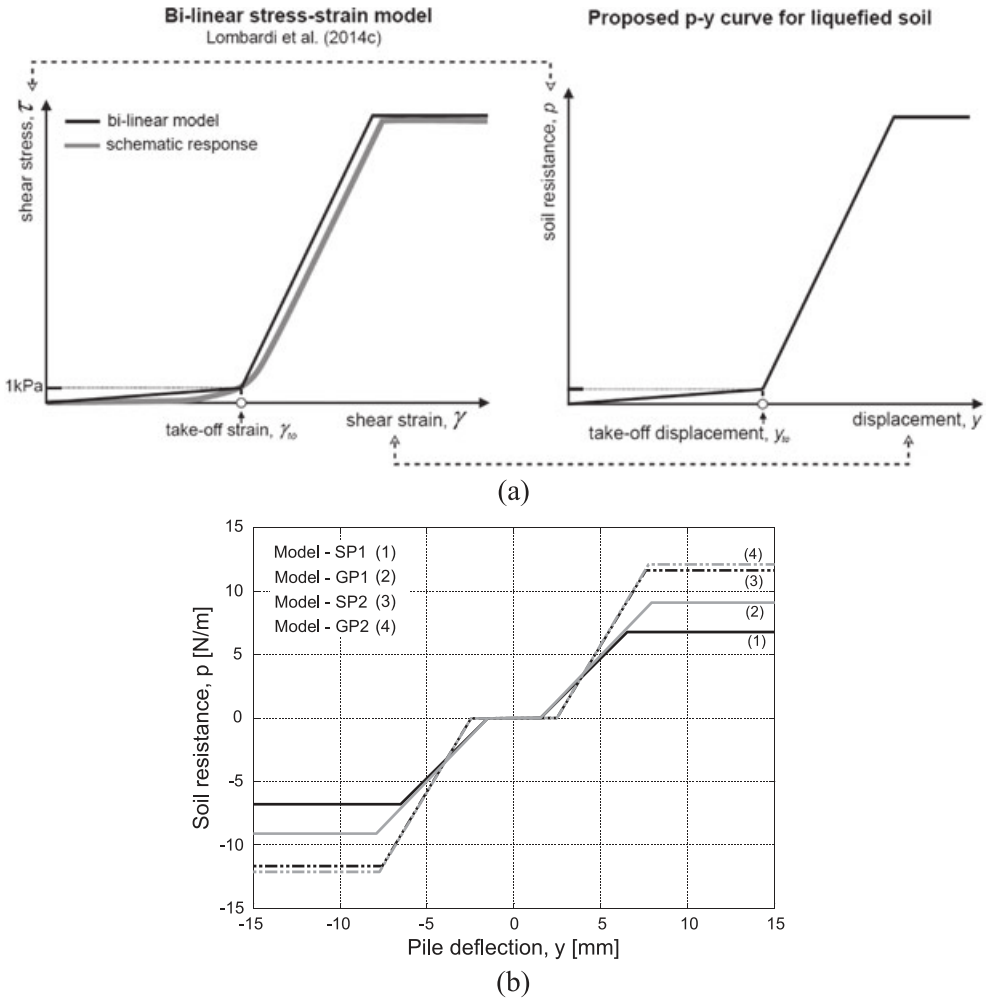

Figure 12. *p–y* curves for liquefied soils: (a) Schematic method for scaling stress–strain into equivalent *p–y* curve; (b) Typical examples of *p–y* curves for liquefied soils proposed in this study.

Table IV. Take-off displacement, y_{to}, used in this study.

Pile diameter, D [mm]	Take-off displacement, y_{to} [mm]
25.4	1.47
41.28	2.38

seismic action is simulated by the application of an equivalent static force that is hereafter referred to as base-shear. For each model, the base-shear is determined from the mass of the pile-cap (listed in Table I) and the value in the pseudo-acceleration response spectrum (Figure 9), which is function of the fundamental period of each model. It is worth noting that the use of pseudo-acceleration spectrum instead of acceleration spectrum is an approximation that is normally adopted in routine practice because the former is directly related to the seismic force. Furthermore, considering the range of fundamental periods and damping of the structures under investigation, the pseudo-acceleration spectrum is practically equal to the acceleration spectrum. A summary of the input parameters is listed in Table V. It can be observed that in transient and full liquefaction conditions each model experiences different pseudo-accelerations, and consequently different base shear, because of two distinct effects resulting from excess pore pressure build-up. These are: (i) lengthening in period or softening response; (ii) variation in pseudo-spectral ordinates (see Figure 9).

DOI: 10.1002/eqe

Table V. Input parameters used for the pseudo-static analysis.

	Transient to liquefaction condition		Full liquefaction condition	
Model ID	Pseudo-acc. [g]	Base-shear [N]	Pseudo-acc. [g]	Base-shear [N]
SP1	0.16	2.98	0.10	1.86
SP2	0.08	6.62	0.05	4.14
GP1	0.18	23.09	0.11	14.11
GP2	0.22	49.03	0.11	24.52

Figure 13 plots the bending moment envelopes in the so-called transient to liquefaction condition. The comparison between computed and experimental bending moment envelopes suggests that the numerical models underestimate the seismic performance of the four models because the experimental values are typically higher than those computed by the analysis. Specifically, the amplification factor, this being defined as ratio between experimental to computed maximum bending moment, ranges from of 2.6 to 5.9 for single pile models SP1 and SP2, respectively; and from 3 to 3.5 for pile-group models GP2 and GP1, respectively. However, it can be observed that this relatively simple procedure is capable of predicting the position of the maximum bending moment with a reasonable accuracy. Figure 14 plots the bending moment envelopes at the full liquefaction condition. These are obtained by using different sets of *p–y* curves that are constructed based on the two methods described in Section 4.2, namely: *p-multiplier* and proposed *p–y* curves. Similarly to the conclusions drawn from Figure 13, the seismic performance of the four models is underestimated because the comparison between computed and measured maximum bending moment indicates that both methods underestimate the experimental values, with no significant differences between the two methods. On the other hand, the proposed method performs better than the conventional *p-multiplier* in replicating the higher bending moments at deeper elevations, which is consistent with real observations made in the field (Hamada, [6]). Although the disparities between experimental and computed values may be attributed to several factors, including model assumptions and *p–y* curves calibration techniques, the trends depicted in Figures 13 and 14 show that the bending moments computed numerically are consistently underestimated by a factor ranging between 2 and 6. It can be argued that this amplification may be caused by potential detrimental effects because of complex soil–foundation interplay (kinematic interaction), which is evidently not taken into account in conventional pseudo-static approaches. A simplified method proposed by the authors consists of applying an amplification factor to the computed bending moments determined by means of pseudo-static methods. In this study, the amplification factor ranges between 2 and 6;

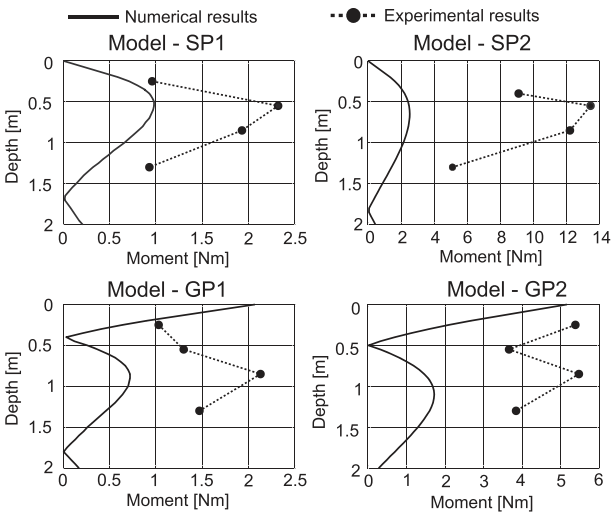

Figure 13. Comparison between computed and measured bending moment envelopes during transient to liquefaction condition.

DOI: 10.1002/eqe

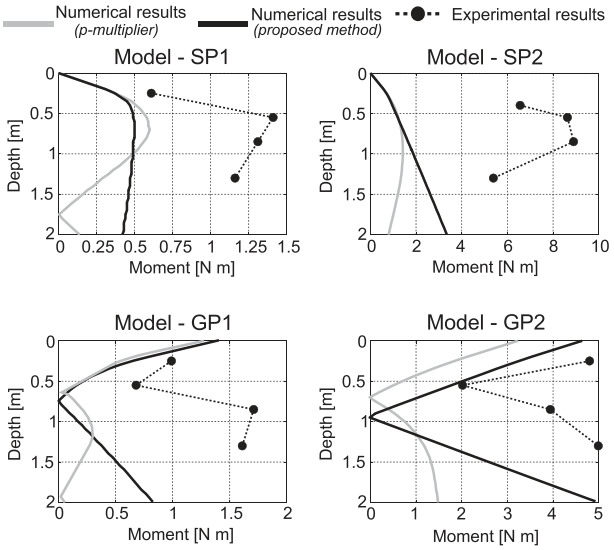

Figure 14. Comparison of computed and measured maximum bending moment envelopes at transient condition.

however, appropriate amplification factors should be computed before applying these to real prototypes. Preliminary results obtained by the authors indicate that the amplification factor is a function of two main parameters, namely: (i) speed of propagation of liquefaction front (i.e. ratio of the liquefiable depth to the time taken to soil liquefaction and it is important to note that ground liquefies top-down) which is predominantly a function of drainage boundary conditions, input motion and soil permeability; (ii) relative magnitude of predominant frequency of the earthquake and natural frequency of the soil–foundation–structure system.

4.4. Capacity-spectrum method: seismic performance based on damage (displacement) criterion

In recent years, a consensus has been reached among the earthquake engineering community to change the attention from '*strength*' to '*performance*'. This has been confirmed by the development of a new generation of design and rehabilitation procedures that form the so-called performance-based engineering (PBE). The primary objective of PBE is to predict the seismic performance of existing and new infrastructures in terms of expected damage to structural and nonstructural components [49]. Differently from the pseudo-static analysis described in Section 4.3, PBE adopts inelastic analysis procedures to compute demand parameters, such as global displacements, storey drift, component distortions, etc., which can be directly used to determine the damage and consequently the seismic performance based on acceptance criteria. In this work, the seismic performance of the four models is computed by adopting the so-called *capacity-spectrum method* (CSM) introduced by Freeman *et al*. [50] and its subsequent variants by Fajfar and Fischinger [51, 52]. The CSM method is based on the basic assumption that the maximum inelastic displacement of each model can be estimated from the maximum deformation of the equivalent linear elastic SDOF oscillator that has larger period and damping than those of the real model listed in Tables II and III [49, 53]. The period of vibration and damping ratio of the equivalent system are commonly referred to as equivalent period and equivalent damping ratio. In spite of the approximations and limitations of the method (see for example Fajfar [54]; Krawinkler & Seneviratna [55]; Krawinkler [56]), it can provide an intuitive assessment of the seismic performance, expressed in terms of global displacement—by means of a graphical comparison between the seismic capacity of the structure and the seismic demand imposed by the earthquake. The final aim of the analysis presented in this section is to evaluate the seismic performance of the four models in terms of maximum global displacement. The seismic capacity of each model is determined from the pushover analysis, whereby each model is subjected to a monotonically increasing horizontal displacement to generate

DOI: 10.1002/eqe

a nonlinear base-shear versus horizontal displacement curve. The latter is hereafter referred to as pushover curve. The seismic capacity of the model is subsequently determined by converting the pushover curve into an equivalent acceleration versus horizontal-displacement curve according to the linearization procedure as documented in FEMA-440 [49]. This conversion enables the capacity curve to be plotted on the same axes as the seismic demand. The seismic demand is expressed in the form of inelastic Acceleration-Displacement-Response-Spectra (ADRS). This is computed based on the acceleration time histories recorded by the accelerometer located 600 mm below the ground level (see Figure 4(b)). According to this approach, the implicit inelastic demand of the ADRS is taken into account by considering an equivalent viscous damping higher than that actually exhibited by the structure and normally used for elastic response spectra. It is worth noting that this is consistent with the well-known hypothesis that the viscous damping is a suitable surrogate for the energy dissipated by hysteretic behaviour of nonlinear system. ATC-40 [53] proposes three equivalent damping levels, i.e. 0.40, 0.29 and 0.20, for hysteretic behaviour types A, B and C, respectively. In this study, an equivalent damping corresponding to hysteretic behaviour type C is used in both transient and full liquefaction conditions because of the relatively low ductility level that one would expect from the four models tested in this study. However, further studies should investigate the correctness of such an assumption.

In spite of using the same equivalent damping for both transient and liquefaction conditions, from Figure 15 it can be seen that the occurrence of liquefaction condition has two distinct effects, namely: (i) it reduces spectral accelerations in the low periods range; this is representative of rigid structures, but it amplifies spectral ordinates for higher periods, i.e. flexible structures. (ii) it reduces the spectral displacements in the low periods range but significantly amplifies the spectral displacements for flexible structures characterised by higher fundamental periods.

The results of the CSM for the transient to liquefaction conditions are depicted in Figure 16. The abscissae of the intersection points of pushover curves (i.e. seismic capacities of the four models) and ADRS curve (i.e. seismic demand imposed by the shaking) identify the displacement demands imposed by the shaking on the four models. As expected, it is found that single pile models SP1 and SP2 exhibit higher displacement demands because of their higher lateral flexibilities when compared to those of pile-group models GP1 and GP2. It is worth noting that there are significant disparities between displacement demands computed according to the CSM and those estimated from recorded measurements (Figure 8). These are likely to be associated to the relative simplicity of the approach used to predict both seismic demand and capacity of the models, which is unable to capture the SSI. During pile–soil interaction in liquefied soil, many physical process and mechanisms take place: complex generation and dissipation of excess pore pressure creating a complex seepage which is induced by variable pore pressure gradient between far-field and soil adjacent to the pile. These are hard to quantify and account for in the simplified analysis, and therefore it is not surprising to see differences between computed and measured displacement demands. Figure 17 depicts the CSM applied to the numerical models at the full liquefaction condition. Similarly to the pseudo-static

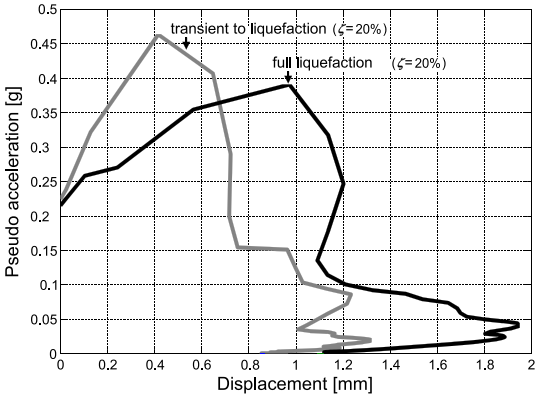

Figure 15. Seismic demand expressed in Acceleration-Displacement-Response-Spectra format for transient and full liquefaction conditions.

DOI: 10.1002/eqe

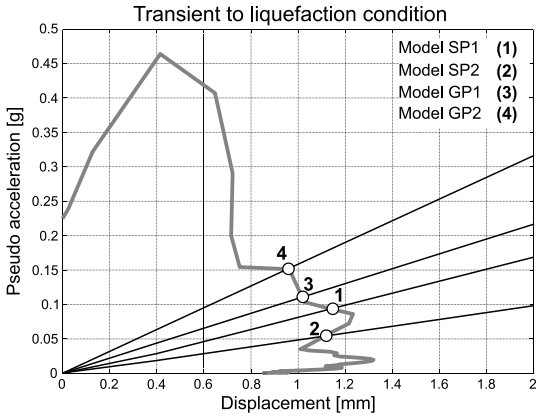

Figure 16. Capacity-spectrum method results: transient to liquefaction condition.

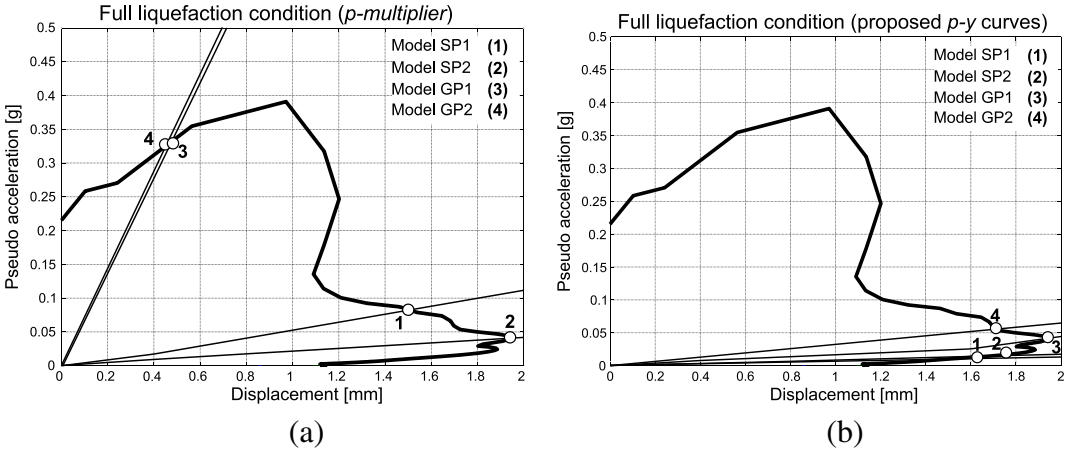

Figure 17. Capacity-spectrum method results at the full liquefaction condition: (a) *p-multiplier*; (b) proposed *p–y* curves.

analysis described in Section 4.3, the effects induced by liquefaction on the SSI are modelled according to the conventional *p-multiplier approach* (Figure 17a) and proposed *p–y* curves (Figure 17b). The comparison in terms of displacement demands shows important differences between the two methods especially for the stiffer pile-group models GP1 and GP2. On the other hand, differently from the transient to liquefaction condition discussed earlier, the displacement demands computed according to the CSM are notably comparable to those estimated from the experimental data (Figure 8). This promising conclusion suggests that the effects induced by the aforementioned transient phenomena have a minor effect on the overall seismic behaviour. All research data supporting this publication are available as supplementary information accompanying this publication at http://dx.doi.org/10.15127/1.296929 [57].

5. CONCLUSIONS

The seismic performance of four typical structures, representing both single-pile and pile-group supported structures, is evaluated in two conditions: transient to liquefaction condition (i.e. $r_u < 1$) and full liquefaction condition (i.e. $r_u = 1$). The seismic performance of each model is evaluated by considering two different criteria consisting of (i) strength criterion expressed in terms of bending moment envelopes along the piles; (ii) damage criterion expressed in terms of maximum global displacement. The effects of liquefaction on SSI are taken into account by considering two families of *p–y* curves: one constructed according to the *p-multiplier* approach and the other proposed by the

DOI: 10.1002/eqe

authors. The latter has the advantage of replicating the strain-hardening behaviour exhibited by the liquefied soil during shearing in the undrained condition. Comparisons between computed and experimentally determined bending moment envelopes show that the numerical models consistently underestimate the seismic response of the structure with no significant differences between the two families of *p–y* curves, although the proposed *p–y* curves better reproduce the redistribution of bending moments to deeper elevations as observed in the real field. It is discussed that this disparity can be related to numerous factors, including model assumptions, *p–y* calibration techniques, boundary conditions, etc. However, it is also argued that this difference may be inherent to the static nature of the analysis, which neglects complex soil–foundation–structure effects and important transient (in both space and time) flow phenomena in the soil adjacent to the foundation.

Furthermore, comparisons between computed and experimentally predicted maximum displacements show that the numerical analysis underestimates the seismic response of the models in the transient to liquefaction condition; however, it provides a remarkably good prediction at the full liquefaction condition when the SSI is modelled through the proposed *p–y* curves. This result is promising because the displacement response is more fundamental to structural damage than strength, especially for piles carrying large axial loads that may become unstable and buckle owing to enhanced P-delta effects caused by lateral displacements.

ACKNOWLEDGEMENTS

The work is partially funded by the EPSRC (Engineering and Physical Sciences Research Council, United Kingdom) through the grant EP/H015345/2. The first author would like to acknowledge the funding received through University of Bristol Centenary PhD Scholarship for 3 years. The second author would also like to acknowledge University of Bristol for the University Senior Research Fellowship for the year 2011 to 2012.

REFERENCES

1. Lombardi D, Bhattacharya S. Liquefaction of soil in the Emilia-Romagna region after the 2012 Northern Italy earthquake sequence. *Natural Hazards* 2014. DOI:10.1007/s11069-014-1168-6.
2. Bhattacharya S, Hyodo M, Goda K, Tazoh T, Taylor C. Liquefaction of soil in the Tokyo Bay area from the 2011 Tohoku (Japan) earthquake. *Soil Dynamics and Earthquake Engineering* 2011; **31**(11):1618–1628.
3. Mylonakis G, Syngros C, Gazetas G, Tazoh T. The role of soil in the collapse of 18 piers of Hanshin expressway in the Kobe earthquake. *Earthquake Engineering & Structural Dynamics* 2006; **35**(5):547–575.
4. Bhattacharya S. Safety assessment of existing piled foundations in liquefiable soils against buckling instability. *ISET Journal of Earthquake Technology* 2006; **43**(4):133–146.
5. Tokimatsu K, Asaka Y. Effects of liquefaction-induced ground displacements on pile performance in the 1995 Nyogoken-Nambu earthquake. *Soils and Foundations* 1998; **2**:163–177.
6. Hamada, M.. Case studies of liquefaction and lifeline performance during past earthquakes. Vol. 1; Japanese case studies, National Center for Earthquake Engineering Research, Technical Report 1992 92, 341.
7. Yoshida, N., Hamada, M.. Damage to foundation piles and deformation pattern of ground due to liquefaction-induced permanent ground deformations. *Proc. Third Japan-US Workshop on Earthquake Resistant Design of Lifeline Facilities and Countermeasures for Soil Liquefaction*, Report NCEER-91-0001', 1991, 141-161.
8. CEN (Comité Européen de Normalisation). *EN 1998-1: Eurocode 8*: *Design of structures for earthquake resistance —Part 1*: *General rules*, *seismic actions and rules for buildings*. CEN: Brussels, Belgium. 2004
9. National Earthquake Hazards Reduction Program (NEHRP). Commentary (Federal Emergency Management Agency, USA, 369) for seismic regulations for new buildings and other structures. 2000
10. IS-1893 Part 1. *Criteria for Earthquake Resistant Design of Structures*. Bureau of Indian Standard: New Delhi, 2000.
11. Lombardi D, Bhattacharya S. Modal analysis of pile-supported structures during seismic liquefaction. *Earthquake Engineering & Structural Dynamics* 2014; **43**(1):119–138.
12. Kamijo N, Saito H, Kusama K, Kontani O, Nigbor R. Seismic tests of a pile-supported structure in liquefiable sand using large-scale blast excitation. *Nuclear Engineering and Design* 2004; **228**(1):367–376.
13. Mylonakis G, Gazetas G. Seismic soil–structure interaction: beneficial or detrimental? *Journal of Earthquake Engineering* 2000; **4**(3):277–301.
14. JRA 2002—Japan Road Association. Specifications for highway bridges, Part V: seismic design, Japan, 2002
15. Knappett JA, Madabhushi SPG. Influence of axial load on lateral pile response in liquefiable soil. Part I: physical modelling. *Geotechnique* 2009; **59**(7):571–581. DOI:10.1680/geo.8.009.3749.
16. Bhattacharya S, Adhikari S, Alexander NA. Simplified method for unified buckling and dynamic analysis of pile supported structures in seismically liquefiable soils. *Soil Dynamics and Earthquake Engineering* 2009; **29**:1220–1235. DOI:10.1016/jsoildyn.2009.01.006.

17. Shaker K, Basudhar PK, Patra NR. Buckling of piles under liquefied soil condition. *Geotechnical and Geological Engineering* 2007; **25**: 303–313. DO1:10.1007/S10706-006-9111-6.
18. Kimura Y, Tokimatsu K. Buckling stress of slender pile with lateral displacement at the pile head in liquefied soils. *Journal of Structural and Construction Engineering. AIJ (Architectural Institute of Japan)* 2007; **617**:169–75.
19. Lin S, Tseng Y, Chiang C, Hung CL. Damage of piles caused by lateral spreading—back study of three cases. *Proc. ASCE Conference on Seismic Performance and Simulation of pile foundation in liquefied and laterally spreading ground*, Davis, University of California, USA: 121-133, 2005.
20. Bhattacharya S, Madabhushi SPG, Bolton MD. An alternative mechanism of pile failure in liquefiable deposits during earthquakes. *Geotechnique* 2004; **54**(3):203–213.
21. CEN (Comité Européen de Normalisation). *EN 1998-5: Eurocode 8: Design of Structures for Earthquake Resistance Part 5*: *Foundations*, *Retaining Structures and Geotechnical Aspects*. CEN: Brussels, Belgium. 2004b.
22. Lombardi D., Durante, M. G., Dash, S. R., Bhattacharya S. Fixity of piles in liquefiable soils. *In Proceedings of 5th International Conference on Recent Advances in Geotechnical Engineering and Soil Dynamics and Symposium in Honor of Professor IM Idriss*. May 24-29, 2010, San Diego, *California*, 2010.
23. Hetényi M. *Beams on Elastic Foundation. Theory with Applications in the Fields of Civil and Mechanical Engineering*. The University of Michigan Press: Ann Arbor, 1946.
24. API. Recommended practice for planning, designing, and constructing fixed offshore platforms—working stress design. 2000
25. DNV. Offshore Standard DNV-OS-J101. *Design of offshore wind turbine structures*. Det Norske Veritas, 2007.
26. Reese, L. C., Cox, W. R., Koop, F. D.. Analysis of laterally loaded piles in sand. *Offshore Technology in Civil Engineering Hall of Fame Papers from the Early Years*, 1974, 95-105.
27. Matlock, H.. Correlations for design of laterally loaded piles in soft clay. *Offshore Technology in Civil Engineering's Hall of Fame Papers from the Early Years*, 1970, 77-94.
28. Dobry, R., Taboada, V., Liu, L.. Centrifuge modelling of liquefaction effects during earthquakes. *Proc. 1st Intl. Conf. On Earthquake Geotechnical Engineering*, IS-Tokyo, 1995, 14-16.
29. Boulanger RW, Kutter BL, Brandenberg SJ, Singh P, Chang D. Pile foundations in liquefied and laterally spreading ground during earthquakes: centrifuge experiments & analyses. *Technical Report, Centre for Geotechnical Modelling, Department of Civil and Environmental Engineering*. University of California, Davis: California, 2003.
30. Wilson DW, Boulanger RW, Kutter BL. Observed seismic lateral resistance of liquefying sand. *Journal of Geotechnical and Geoenvironmental Engineering* 2000; **126**(10):898–906.
31. Boulanger RW, Wilson DW, Kutter BL, Abghari A. Soil–pile superstructure interaction in liquefiable sand. *Transportation Research Record: Journal of the Transportation Research Board* 1997; **1569**(1):55–64.
32. Cubrinovski M, Kokusho T, Ishihara K. Interpretation from large scale shake table tests on piles undergoing lateral spreading in liquefied soils. *Soil Dynamics and Earthquake Engineering* 2006; **26**(2):275–286.
33. Brandenberg SJ, Boulanger RW, Kutter BL, Chang D. Static pushover analyses of pile groups in liquefied and laterally spreading ground in centrifuge tests. *Journal of Geotechnical and Geoenvironmental Engineering* 2007; **133**(9):1055–1066.
34. AIJ. Architectural Institute of Japan. *Recommendations for design of building foundations* (in Japanese). 2001.
35. Finn WL. A study of piles during earthquakes: issues of design and analysis. *Bulletin of Earthquake Engineering* 2005; **3**(2):141–234.
36. Goh, S., O'Rourke, T.. Limit state model for soil–pile interaction during lateral spread. *Proc. of 7th US Japan workshop on earthquake resistant design of lifeline facilities and countermeasures against soil liquefaction*. Seattle, WA. 1999.
37. Seed RB, Harder L. SPT-based analysis of cyclic pore pressure generation and undrained residual strength. *Proc. of the H. Bolton Seed memorial symposium* 1990; **2**:351–376.
38. Lombardi D, Bhattacharya S, Hyodo M, Kaneko T. Undrained behaviour of two silica sands and practical implications for modelling SSI in liquefiable soils. *Soil Dynamics and Earthquake Engineering* 2014; **66**:293–304.
39. Dash S. Lateral pile–soil interaction in liquefiable soils, *Ph.D. Thesis*, University of Oxford. UK., 2010.
40. Tokimatsu, K., Suzuki, H. Suzuki, Y.. Back-calculated p–y relation of liquefied soils from large shaking table tests. *Proc. 4th International Conf. on Recent Advances in Geotechnical Earthquake Engineering and Soil Dynamics*. 2001, 1-6.
41. Wilson D. W. Soil–pile–superstructure interaction in liquefying sand and soft clay, *Ph.D. Thesis*, University of California, Davis. 1998
42. Lombardi D, Bhattacharya S, Scarpa F, Bianchi M. Dynamic response of a geotechnical rigid model container with absorbing boundaries. *Soil Dynamics and Earthquake Engineering* 2015; **69**:46–56.
43. Seed HB, Idriss IM. Simplified procedure for evaluating soil liquefaction potential'. *Journal of the Soil Mechanics and Foundations Division* 1971; **97**(9):1249–1273.
44. Worden K, Tomlinson GR. *Nonlinearity in Structural Dynamics: Detection, Identification and Modelling*. Institute of Physics Publishing, Bristol, UK, 2000.
45. Chopra, A. K.. Dynamics of structures. Prentice-Hall International Series in Civil Engineering and Engineering Mechanics. 1995.
46. CSI. SAP2000, V14. *Integrated Software for Structural Analysis and Design*. Berkeley, CA, USA: Computer and Structures Inc.(CSI). 2009.

DOI: 10.1002/eqe

47. Lombardi D. Dynamics of pile-supported structures in seismically liquefiable soils. *Ph.D. Thesis*. University of Bristol. UK. 2013.
48. Bouzid D, Dash S.R, Bhattacharya S. Winkler Springs (p–y curves) for pile design from stress–strain of soils: FE assessment of scaling coefficients using the Mobilized Strength Design concept, *Geomechanics and Engineering* 2013, DOI: 10.12989/gae.2013.5.5.379
49. FEMA-440. *Improvement of Nonlinear Static Seismic Analysis Procedures, Applied Technology Council (ATC-55 Project)*. Federal Emergency Management agency: Washington, DC, 2005.
50. Freeman S., Nicoletti J., Tyrell J. Evaluations of existing buildings for seismic risk—a case study of Puget sound naval shipyard, Bremerton, Washington. *Proc. of the 1st US National Conference on Earthquake Engineering*. 1975, 113-122.
51. Fajfar P, Fischinger M. N2-A method for non-linear seismic analysis of regular buildings. *Proc. of the Ninth World Conference in Earthquake Engineering* 1989; **5**:111–116.
52. Fajfar P, Fischinger M. Non-linear seismic analysis of RC buildings: implications of a case study. *European Earthquake Engineering* 1987; **1**(1):31–43.
53. ATC-40. Applied Technology Council: *Seismic evaluation and retrofit of concentre buildings*. Applied Technology Council, report SSC96-01. Redwood City, California, 1996.
54. Fajfar P. A nonlinear analysis method for performance-based seismic design. *Earthquake Spectra* 2000; **16**(3):573–592.
55. Krawinkler H, Seneviratna GDPK. Pros and cons of a pushover analysis of seismic performance evaluation. *Engineering Structures* 1998; **20**(4):452–464.
56. Krawinkler H. New trends in seismic design methodology. *Proc. the 10th European Conference on Earthquake Engineering*, Vol. 2, Vienna, 1994, Balkema, Rotterdam, 2, 1995, 821-830.
57. Lombardi D Bhattacharya S. *Shaking table data*. The University of Manchester http://dx.doi.org/10.15127/1.296929

DOI: 10.1002/eqe